

# Causal Inference via Style Transfer for Out-of-distribution Generalisation

Toan Nguyen  
s222165627@deakin.edu.au  
Applied Artificial Intelligence  
Institute, Deakin University  
Australia

Kien Do  
k.do@deakin.edu.au  
Applied Artificial Intelligence  
Institute, Deakin University  
Australia

Duc Thanh Nguyen  
duc.nguyen@deakin.edu.au  
School of Information Technology,  
Deakin University  
Australia

Bao Duong  
duongng@deakin.edu.au  
Applied Artificial Intelligence  
Institute, Deakin University  
Australia

Thin Nguyen  
thin.nguyen@deakin.edu.au  
Applied Artificial Intelligence  
Institute, Deakin University  
Australia

## ABSTRACT

Out-of-distribution (OOD) generalisation aims to build a model that can generalise well on an unseen target domain using knowledge from multiple source domains. To this end, the model should seek the causal dependence between inputs and labels, which may be determined by the semantics of inputs and remain invariant across domains. However, statistical or non-causal methods often cannot capture this dependence and perform poorly due to not considering spurious correlations learnt from model training via unobserved confounders. A well-known existing causal inference method like back-door adjustment cannot be applied to remove spurious correlations as it requires the observation of confounders. In this paper, we propose a novel method that effectively deals with hidden confounders by successfully implementing front-door adjustment (FA). FA requires the choice of a mediator, which we regard as the semantic information of images that helps access the causal mechanism without the need for observing confounders. Further, we propose to estimate the combination of the mediator with other observed images in the front-door formula via style transfer algorithms. Our use of style transfer to estimate FA is novel and sensible for OOD generalisation, which we justify by extensive experimental results on widely used benchmark datasets.

## CCS CONCEPTS

• **Computing methodologies** → **Causal reasoning and diagnostics; Learning under covariate shift; Computer vision.**

## KEYWORDS

Causal Inference; Out-of-distribution Generalisation; Domain Generalisation; Style Transfer

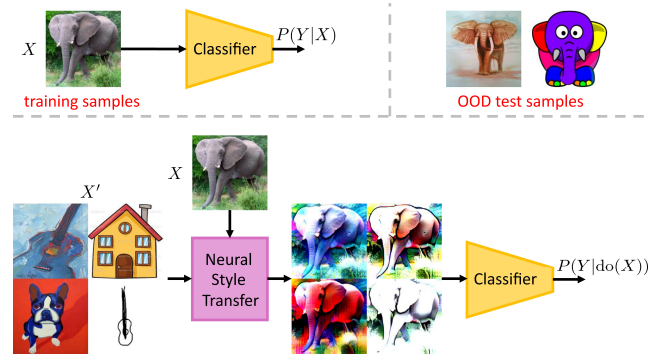


**Figure 1: A model of  $P(Y|X)$  (top) tends to capture all associations between  $X$  and  $Y$  including the spurious dependence while a model of  $P(Y|do(X))$  (bottom) only captures the causal dependence  $X \rightarrow Y$ .  $P(Y|do(X))$  can be identified via front-door adjustment by leveraging style transfer in our method.**

## ACM Reference Format:

Toan Nguyen, Kien Do, Duc Thanh Nguyen, Bao Duong, and Thin Nguyen. 2023. Causal Inference via Style Transfer for Out-of-distribution Generalisation. In *Proceedings of the 29th ACM SIGKDD Conference on Knowledge Discovery and Data Mining (KDD '23)*, August 6–10, 2023, Long Beach, CA, USA. ACM, New York, NY, USA, 19 pages. <https://doi.org/10.1145/3580305.3599270>

## 1 INTRODUCTION

A common learning strategy in image classification is to maximise the likelihood of the conditional distribution  $P(Y|X)$  of a class label  $Y$  given an input image  $X$  over a training set. This objective is performed by exploiting the statistical dependence between input images and class labels in the training set to yield good predictions on a test set. Although this learning strategy works well for the “in-distribution” setting in which the test and training sets are from the same domain, recent works [1, 29, 55] have pointed out its limitations in dealing with out-of-distribution (OOD) samples. This deficiency acts as a significant barrier to real-world applications, where the test data may come from various domains and may follow different distributions.

Permission to make digital or hard copies of all or part of this work for personal or classroom use is granted without fee provided that copies are not made or distributed for profit or commercial advantage and that copies bear this notice and the full citation on the first page. Copyrights for components of this work owned by others than the author(s) must be honored. Abstracting with credit is permitted. To copy otherwise, or republish, to post on servers or to redistribute to lists, requires prior specific permission and/or a fee. Request permissions from [permissions@acm.org](mailto:permissions@acm.org).

KDD '23, August 6–10, 2023, Long Beach, CA, USA

© 2023 Copyright held by the owner/author(s). Publication rights licensed to ACM.

ACM ISBN 979-8-4007-0103-0/23/08...\$15.00

<https://doi.org/10.1145/3580305.3599270>

The OOD generalisation task [13, 46] aims to address the issue by requiring deep learning models to infer generalisable knowledge, which can be discovered by seeking the true causation of labels or the causal dependence between inputs and labels [1, 43, 44]. However, owing to causal inference, statistical correlations in training data do not always imply the true causation of features to labels [11, 44, 61]. On the other hand, *domain-specific nuisance features* that are variant across domains can be learnt via statistical correlations [1, 7, 29]. These features are captured incidentally from confounding factors such as background, or viewpoint, which change across domains and confound the causal dependence between images and labels. For example, when most training images of the elephant class are found with grass (Fig. 1), by statistical learning, a deep learning model is prone to taking into account features from the grass (e.g., the green colour) as a signature for the elephant class. This bias would mislead the model to wrong predictions on test data from a different domain (e.g., when an elephant appears on a stage or in a sketch painting). Here, by observing the statistical dependence between the grass and the elephant class, one cannot conclude either one of them is the cause of the other. Technically, a model, which learns by the statistical correlation objective  $P(Y|X)$  on a specific domain, might capture the spurious dependence induced by confounders from that domain, leading to inferior generalisation ability.

Intuitively, we should model only the true causal dependence between  $X$  and  $Y$ . In causal inference literature, such dependence is represented as  $P(Y|\text{do}(X))$ . Here, the  $\text{do}(X)$  operator means an intervention on  $X$ , which allows us to remove all spurious associations between  $X$  and  $Y$  [11, 44].  $P(Y|\text{do}(X))$  can be estimated via back-door adjustment [11]. However, a well-known drawback of this approach is the need for observable confounders. This requirement is not realistic and confounders are also hard to be explicitly modelled (e.g., decomposing domain background variables) [11, 53]. An alternative approach to the issue is front-door adjustment (FA) [11, 44], which supports causal inference with hidden confounders, making the problem setting more practical. Implementation of FA requires the choice of a mediator, which we regard as the *semantic information of images* that helps access the causal dependence, in other words, features extracted from images that are *always* predictive of labels. Further, the front-door formula appeals to a feasible way of modelling the combination of the class-predictive semantics of an input image with the style and/or context of other images. Such capability is naturally supported by style transfer models as illustrated in Fig. 1. These methods have demonstrated their ability to not only transfer artistic styles but also effectively capture the semantic content of images [15, 58, 65], which we propose that they hold promise for fulfilling the front-door requirements. In this work, we propose a novel front-door adjustment-based method to learn the causal distribution  $P(Y|\text{do}(X))$  in OOD generalisation. We realise our method using two different style transfer models: AdaIN Neural Style Transfer (NST) [15] and Fourier-based Style Transfer (FST) [58]. Our use of style transfer to estimate FA is novel and sensible for OOD generalisation, which we show via the superior generalisation capacity of our model on widely used benchmark datasets. In summary, our main contributions include:

- A formulation of OOD generalisation under the perspective of causal inference;
- A causal inference solution to OOD generalisation based on FA, which we successfully implemented by two different style transfer strategies. Our source code is available at: <https://github.com/nktoan/Causal-Inference-via-Style-Transfer-for-OOD-Generalisation>.
- Extensive experiments on various benchmark datasets, showing the superiority of our proposed algorithm over state-of-the-art OOD generalisation methods.

## 2 RELATED WORK

**Causal Inference** has been a fundamental research topic. It aims to reconstruct causal relationships between variables and estimate causal effects on variables of interest [11, 61]. Causal inference has been applied to many deep learning research problems, especially in domain adaptation (DA) [30, 42, 62, 64] and domain generalisation (DG) [31, 35, 55]. However, various difficulties curtail its development in deep learning. The most common application of causal inference is removing spurious correlations of domain-specific confounders that affect the generalisation ability of deep models [27, 60]. Existing methods often adopt back-door adjustment to derive the causal dependence. Examples include visual grounding [14], semantic segmentation [63], and object detection [56]. However, in practice, confounders may not be always observed. In addition, they are hard to be derived [11, 53]. In this case, front-door adjustment (FA) [11, 39] is often preferred. FA makes use of a mediator variable to capture the intermediate causal effect. The effectiveness of the FA approach has also been verified in many tasks such as vision-language tasks [60], image captioning [59], and DG [27]. The main difference between our front-door-based algorithm and others is the interpretation of the front-door formula in causal learning. To the best of our knowledge, the incarnation of style transfer algorithms [15, 20, 26] in FA is novel. It is a sensible and effective way for DG, which is proven by our experimental results. Besides, to deal with hidden confounders, instrumental [2, 49] or proxy [34, 62] variables can also be used. However, in the DG problem, identifying the appropriate mediator variable for FA presents fewer challenges and offers greater practicality compared to selecting instrumental or proxy variables. Causal inference methods are not straightforward to be technically implemented for practical computer vision tasks. Our work can be seen as the first attempt to effectively apply FA via style transfer algorithms for DG.

**Domain Generalisation (DG)** aims to build image classification models that can generalise well to unseen data. Typical DG methods can be divided into three approaches including domain-invariant features learning [37, 40], meta-learning [8, 23, 27, 66], and data/feature augmentation [16, 69, 71]. Domain-invariant features can be learnt from different source distributions via adversarial learning [25, 28, 36], domain alignment [37, 67], or variational Bayes [57]. Meta-learning addresses the DG problem by simulating domain shift, e.g., by splitting data from source domains into pseudo-training and pseudo-test data [22]. Data/feature augmentation [55, 69] can be used to improve OOD generalisation by enhancing the diversity of learnt features. Instead of seeking domain-invariant features, our method aims to learn the causal mechanism

between images and targets, which is robust and invariant against domain shift [1, 27, 29]. Among data augmentation methods, our method is related to MixStyle [71] and EFDMix [65] due to the use of style transfer (i.e., the AdaIN algorithm [15]) to create novel data samples. However, our method considers preserving the content of images as it is crucial in causal learning. Meanwhile, MixStyle only interleaves some style transfer layers into image classification models. In addition, both MixStyle and EFDMix rely on statistical predictions, which are sensitive to domain shift [1, 32]. More, we regard the AdaIN algorithm as a tool to implement our proposed front-door formula for estimating the causal dependence, resulting in generalisable predictions. Similarly, the key advantage of our method over FACT [58] is that we use the Fourier-based transformation as an implementation of style transfer to infer the causal dependence.

**Causal Inference for DG.** The connection between causality and DG has recently drawn considerable attention from the research community. Much of the current line of work relies on the assumption that there exists causal mechanisms or dependences between inputs or input features and labels, which will be invariant across domains [1, 9, 29, 32, 50]. Many causality-inspired approaches [17, 29, 31, 55] learn the domain-invariant representation or content feature that can be seen as a direct cause of the label. Owing to the principle of invariant or independent causal mechanisms [35, 41, 44], the causal mechanism between the content feature and the label remains unchanged regardless of variations in other variables, such as domain styles. Some methods [29, 35, 55] enforce regularisation with different data transformations on the learnt feature to achieve the content feature. For example, CIRL [29] performs causal intervention via Fourier-based data augmentation [58]. On the other hand, MatchDG [31] assumes a causal graph where the content feature is independent of the domain given the hidden object and proposes a method that enforces this constraint to the classifier by alternately performing contrastive learning and finding good positive matches. One drawback of MatchDG is its reliance on the availability of domain labels. Causal mechanism transfer [50] aims to capture causal mechanisms for DA via nonlinear independent component analysis [18]. Asides, TCM [62] leverages the proxy technique [34, 62] to perform causal inference for DA (where the target domain is provided) rather than DG.

In contrast, our method postulates that the causal dependence between inputs and labels in DG can be identified by removing spurious correlations induced by *hidden* confounders [11]. On the other hand, some methods [17, 29] assume that there is no confounding variable in their proposed causal graph, which might be unlikely to be satisfied as proposed in many previous methods [19, 48]. An advantage of our approach over the above methods is that we do not rely on imposing regularisation objectives, which may have gradient conflicts with other learning objectives [4]. Our method proposes to use the FA theorem [11, 39] and estimate the front-door formula via style transfer algorithms [15, 20, 26]. Note that CICF [27] also removes spurious correlations using the FA theorem. However, while CICF deploys a meta-learning algorithm to compute the front-door formula, we interpret the formula via style transfer, which generates counterfactual images for causal learning.

### 3 PROBLEM FORMULATION

Let  $X$  and  $Y$  be two random variables representing an input image and its label, respectively. Statistical machine learning methods for image classification typically model the observational distribution  $P(Y|X)$ . They often perform well in the “in-distribution” (ID) setting where both training and test samples are from the same domain. However, they may not generalise well in “out-of-distribution” (OOD) setting where test samples are from an unseen domain. As we will show below, a possible reason for this phenomenon is that  $P(Y|X)$  is *domain-dependent* while a proper model for OOD generalisation should be *domain-invariant*.

#### 3.1 Out-of-Distribution Generalisation under the Causal Inference Perspective

In order to clearly understand the limitation of statistical learning in the OOD setting, we analyse the distribution  $P(Y|X)$  under the causality perspective. In Fig. 2(a), we consider a causal graph  $\mathcal{G}$  which describes possible relationships between  $X$  and  $Y$  in the context of OOD generalisation. In this graph, besides  $X$  and  $Y$ , we also have two other random variables  $D$  and  $U$  respectively specifying the *domain-specific* and *domain-agnostic* features that influence both  $X$  and  $Y$ .  $D$  and  $U$  are unobserved since, in practice, their values are rarely given during training and can only be inferred from the training data. All connections between  $X$  and  $Y$  in  $\mathcal{G}$  are presented below.

- $X \rightarrow Y$  : This is the *true causal relationship* between  $X$  and  $Y$  that describes how the *semantics* in an image  $X$  lead to the prediction of a label  $Y$ .
- $X \leftarrow D \rightarrow Y$  : This is a *spurious relationship* showing that some *domain-specific features*  $D$  can act as a confounder that distorts the true causal relationship between  $X$  and  $Y$ . Different domains usually have different distributions for  $D$ . As a result, if a model relies on  $D$  to predict labels during training, that model would generalise poorly to an OOD test domain. An example of this confounding dependence is that most “giraffe” images from the “art-painting” domain are drawn with a specific texture, and a model trained on these samples may associate the texture with the class “giraffe”.
- $X \leftarrow U \rightarrow Y$  : This is another *spurious relationship* specifying the confounding dependence between  $X$  and  $Y$  caused by *domain-agnostic features*  $U$ . For example, since most elephants are gray, a model may misuse this colour information to predict a dog in gray as an elephant. Here, “gray” is an inherent property of elephants and may not depend on domains.

According to the graph  $\mathcal{G}$ , the statistical distribution  $P(Y|X = x)$  has the following mathematical expression:

$$P(Y|x) = \sum_{d,u} p(d, u|x) P(Y|x, d, u) \quad (1)$$

$$= \mathbb{E}_{p(d,u|x)} [P(Y|x, d, u)] \quad (2)$$

where  $d, u$  denote specific values of  $D, U$  respectively. Here, we make a slight notation abuse by using  $\sum$  as an integral operator. We can see that  $P(Y|x)$  is comprised of the *causal* and *spurious relationships* which correspond to  $x, d$  and  $u$  in  $P(Y|x, d, u)$ . Since  $p(d, u|x)$  can be different for different  $x$ , a model of  $P(Y|x)$  is likely

biased towards some domain-specific and domain-agnostic features  $d, u$ . Therefore, in an unseen test domain,  $P(Y|x)$  tends to make wrong label predictions.

Naturally, we are interested in a model that *captures only the true causal relationship* between  $X$  and  $Y$ . From the perspective of causal inference, we should model  $P(Y|\text{do}(x))$  rather than  $P(Y|x)$ .  $\text{do}(x)$  or  $\text{do}(X = x)$  is a notation from the do-calculus [11] meaning that we intervene  $X$  by setting its value to  $x$  regardless of the values of  $U$  and  $D$ . Graphically, the intervention  $\text{do}(x)$  removes all incoming links from  $D, U$  to  $X$ , blocking all associative paths from  $X$  to  $Y$  except for the direct causal path  $X \rightarrow Y$ .  $P(Y|\text{do}(x))$  is, therefore, regarded as the distribution of the potential outcome  $Y$  under the intervention  $\text{do}(x)$ .

**Maximum Interventional Log-likelihood.** If we can devise a parametric model  $P_\theta(Y|\text{do}(x))$  of  $P(Y|\text{do}(x))$  using observational training data  $\mathcal{D}$ , we can train this model by optimizing the following objective:

$$\theta^* = \underset{\theta}{\operatorname{argmax}} \mathbb{E}_{(x,y) \sim \mathcal{D}} [\log P_\theta(Y = y|\text{do}(x))] \quad (3)$$

We refer to the objective in Eq. (3) as *Maximum Interventional Log-likelihood (MIL)* to distinguish it from the conventional Maximum Log-likelihood (ML) for  $P(Y|x)$ . We note that Eq. (3) makes use of the *consistency* and *no-interference assumptions* [61] in causal inference. The former states that the observed outcome  $y$  of an observed treatment  $X = x$  is the potential outcome of  $Y$  under the intervention  $\text{do}(X = x)$ , and the latter states that the potential outcome  $Y_i$  of an item (or sample)  $i$  is only affected by the intervention on this item (or  $\text{do}(X_i = x)$ ). Detailed derivations of Eq. (3) are provided in the supplementary material. For the ease of notation, we use  $P(Y|\text{do}(x))$  hereafter to denote a parametric model of the potential outcome  $Y$ .

### 3.2 Identification via Back-door Adjustment

Given the appeal of modelling  $P(Y|\text{do}(x))$  for OOD generalisation, the next question is “Can we identify this causal distribution?”, or more plainly, “Can we express  $P(Y|\text{do}(x))$  in terms of conventional statistical distributions?”. A common approach to identify  $P(Y|\text{do}(x))$  is using the *back-door adjustment* as below:

$$P(Y|\text{do}(x)) = \sum_{d,u} p(d,u) P(Y|x, d, u) \quad (4)$$

However, this back-door adjustment is only applicable if  $D$  and  $U$  are observed. In the case  $D$  and  $U$  are unobserved as specified in the graph  $\mathcal{G}$ , there is no way to estimate  $p(d, u)$  in Eq. (4) without using  $x$ . Therefore, there is a need for another approach to identify  $P(Y|\text{do}(x))$ .

## 4 PROPOSED METHOD

We present our proposed front-door adjustment-based method for modelling  $P(Y|\text{do}(x))$  to deal with hidden confounders in Section 4.1 and introduce two different ways to estimate it for OOD image classification in Section 4.2 and Section 4.3.

### 4.1 Identification via Front-door Adjustment

In order to use front-door adjustment, we assume that there is a random variable  $Z$  acting as a mediator between  $X$  and  $Y$  as illustrated in Fig. 2(b).  $Z$  must satisfy three conditions as follows [11]: (i) All directed paths from  $X$  to  $Y$  flow through  $Z$ . (ii)  $X$  blocks all back-door paths from  $Z$  to  $Y$ . (iii) There are no unblocked back-door paths from  $X$  to  $Z$ .

The first two conditions suggest that  $Z$  should capture all and only semantic information in  $X$  that is always predictive of  $Y$ , while the last condition means that we should be able to estimate the causal relationship  $X \rightarrow Z$  by using just the observed training images. Such variable  $Z$  can be captured by several learning methods, such as style transfer models [15, 20] or contrastive learning [31, 53]. Even if the assumptions do not hold perfectly in practice and the mediator captures some spurious features in  $X$ , our method simply reverts to the standard empirical risk minimisation (ERM) model [51], which is widely applicable and can be used on any dataset or problem. Importantly, the more semantically meaningful information that the mediator  $Z$  captures from  $X$ , the better our method can approximate  $P(Y|\text{do}(x))$ . We refer the reader to our supplementary material for a proof sketch that  $Z$  as semantic features will satisfy all the front-door criteria. Given the above conditions, we can determine  $P(Y|\text{do}(x))$  via front-door adjustment as follows:

$$P(Y|\text{do}(x)) = \sum_z p(z|\text{do}(x)) P(Y|z, \text{do}(x)) \quad (5)$$

$$= \sum_z p(z|x) P(Y|\text{do}(z), \text{do}(x)) \quad (6)$$

$$= \sum_z p(z|x) P(Y|\text{do}(z)) \quad (7)$$

$$= \sum_z p(z|x) \left( \sum_{x'} p(x') P(Y|z, x') \right) \quad (8)$$

$$= \mathbb{E}_{p(z|x)} \mathbb{E}_{p(x')} [P(Y|z, x')] \quad (9)$$

where  $z, x'$  denote specific values of  $Z$  and  $X$ , respectively. Detailed derivations of all steps in Eq. (9) are provided in the supplementary material.

One interesting property of the final expression in Eq. (9) is that the label prediction probability  $P(Y|z, x')$  no longer depends on the domain-specific and domain-agnostic features  $D$  and  $U$  unlike  $P(Y|x, d, u)$  in the back-door adjustment formula in Eq. (4). It suggests that by using front-door adjustment, we can explicitly handle the OOD generalisation problem. In addition, the final expression is elegant as the two expectations can be easily estimated via Monte Carlo sampling and  $p(z|x)$  can be easily modelled via an encoder that maps  $x$  to  $z$ . The only remaining problem is modelling  $P(Y|z, x')$ . In the next section, we propose a novel way to model  $P(Y|z, x')$  in front-door adjustment by leveraging neural style transfer.

### 4.2 Front-door Adjustment via Neural Style Transfer

The main difficulty of modelling  $P(Y|z, x')$  is designing a network that can combine the semantic features  $z$  of an image  $x$  with another image  $x'$  without changing the class-predictive semantic information in  $z$ . Here, we want a model that can fuse the content of  $x$



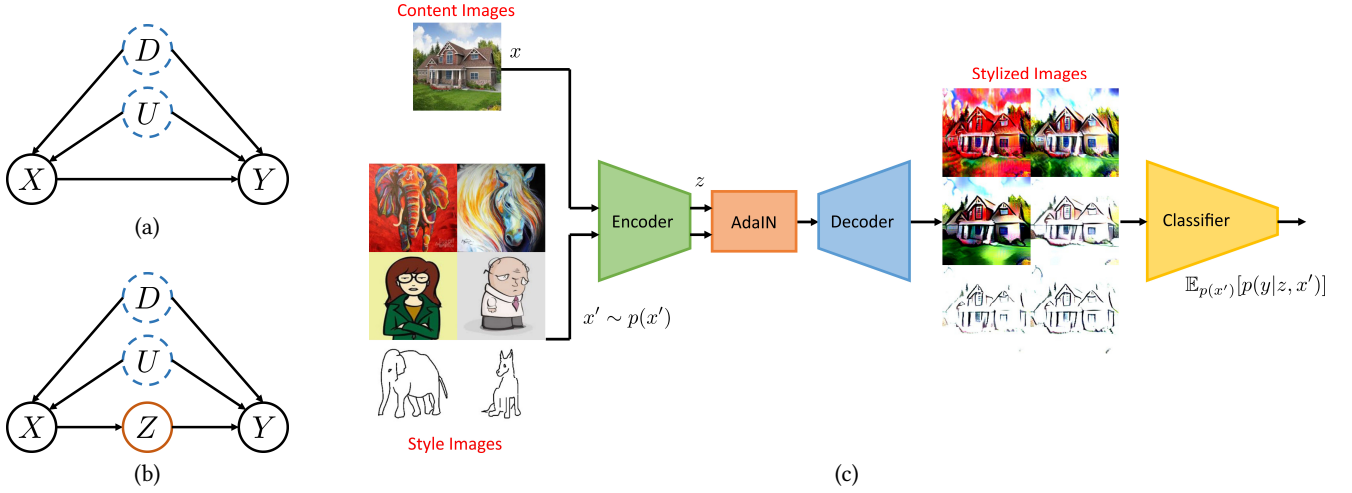


**Figure 2: (a): A causal graph  $\mathcal{G}$  describing the *causal relationship*, *domain-specific association* (via  $D$ ), and *domain-agnostic association* (via  $U$ ) between an input image  $X$  and a label  $Y$ . Variables with dashed border ( $D$ ,  $U$ ) are unobserved. (b): A variant of  $\mathcal{G}$  with a mediator  $Z$  between  $X$  and  $Y$  that enables identification of  $P(Y|\text{do}(x))$  via front-door adjustment. (c): Illustration of our proposed method that leverages style transfer models [15, 58] to perform front-door adjustment.**

with the style of  $x'$ . A family of models that has such capability is neural style transfer (NST). Within the scope of this paper, we consider AdaIN NST [15] as a representative NST method and use it to model  $P(Y|z, x')$ . We note that it is straightforward to use other NST methods, e.g., [65] in place of AdaIN NST. We refer this version to as FAST (*Front-door Adjustment via Style Transfer*). Below, we describe AdaIN NST and the training objective of our method.

An AdaIN NST model consists of an encoder  $E$ , an AdaIN module, and a decoder  $D$  as shown in Fig. 2(c). The encoder  $E$  maps a content image  $x$  and a style image  $x'$  to their corresponding feature vectors  $z = E(x)$  and  $z' = E(x')$ , respectively. The content and style features  $z, z'$  then serve as inputs to the AdaIN module to produce a *stylised feature*  $\tilde{z}$  as follows:

$$\tilde{z} = \text{AdaIN}(z, z') = \mu(z') + \sigma(z') \frac{z - \mu(z)}{\sigma(z)} \quad (10)$$

where  $\mu(z)$ ,  $\sigma(z)$  denote the mean and standard deviation vectors of  $z$  along its channel; so as  $\mu(z')$ ,  $\sigma(z')$  for  $z'$ . Specifically, if  $z$  is a feature map of shape  $C \times H \times W$  with  $C, H, W$  being the number of channels, height, and width, then  $\mu(z)$ ,  $\sigma(z)$  are computed as follows:

$$\mu_c(z) = \frac{1}{HW} \sum_{h=1}^H \sum_{w=1}^W z_{c,h,w}, \quad (11)$$

$$\sigma_c(z) = \sqrt{\frac{1}{HW-1} \sum_{h=1}^H \sum_{w=1}^W (z_{c,h,w} - \mu_c(z))^2} \quad (12)$$

For better controlling the amount of style transferred from  $x'$  to  $x$ , we perform a linear interpolation between  $\tilde{z}$  and  $z$ , then set the result back to  $\tilde{z}$  as follows:

$$\tilde{z} \leftarrow \alpha \tilde{z} + (1 - \alpha)z \quad (13)$$

where  $0 \leq \alpha \leq 1$  is the interpolation coefficient. The stylised code  $\tilde{z}$  in Eq. (13) is sent to the decoder  $D$  to generate a *stylised image*

$\tilde{x} = D(\tilde{z})$ . In summary, we can write  $\tilde{x}$  as a function of  $x$  and  $x'$  in a compact form below:

$$\tilde{x} = \text{AdaIN\_NST}(x, x') \quad (14)$$

where  $\text{AdaIN\_NST}(\cdot, \cdot)$  denotes the AdaIN NST model described above. We can easily substitute  $\text{AdaIN\_NST}$  by other NST methods to compute  $\tilde{x}$  from  $x$  and  $x'$ .

Once the AdaIN NST model has been learnt well,  $\tilde{x}$  will capture the semantic feature  $z$  of  $x$  and the style of  $x'$  properly. Thus, we can condition  $Y$  on  $\tilde{x}$  instead of  $z$  and  $x'$  and regard  $\mathbb{E}_{p(x')} [P(Y|\tilde{x})]$  as an approximation of  $\mathbb{E}_{p(z|x)} \mathbb{E}_{p(x')} [P(Y|z, x')]$ . We compute the label of  $\tilde{x}$  by feeding this stylised image through the classifier  $F$ .

We train  $F$  using the Maximum Interventional Likelihood criterion described in Section 3.1. The loss w.r.t. each training sample  $(x, y)$  is given below:

$$\mathcal{L}_{\text{FAST}}(x, y) = -\log P(Y = y | \text{do}(x)) \quad (15)$$

$$= \mathcal{L}_{\text{xent}} \left( \mathbb{E}_{p(x')} [F(\tilde{x})], y \right) \quad (16)$$

$$= \mathcal{L}_{\text{xent}} \left( \left( \frac{1}{K} \sum_{k=1}^K F(\tilde{x}_k) \right), y \right) \quad (17)$$

where  $F(\cdot)$  denotes the class probability produced by  $F$  for an input image,  $\mathcal{L}_{\text{xent}}$  denotes the cross-entropy loss, and  $\tilde{x}$  is derived from  $x$  and  $x'$  via Eq. (14). The RHS of Eq. (17) is the Monte Carlo estimate of the counterpart in Eq. (16) with  $K$  the number of style images  $x'_1, \dots, x'_K$  and  $\tilde{x}_k = \text{AdaIN\_NST}(x, x'_k)$ . Due to the arbitrariness of the style images  $\{x'\}$ , the stylised images  $\{\tilde{x}\}$  can have large variance despite sharing the same content  $x$ . We found that the large variance of  $\{\tilde{x}\}$  can make the learning fluctuating. To avoid this, we combine the label predictions of  $K$  stylised images with

that of the content image, and use a loss:

$$\mathcal{L}_{\text{FAST}}(x, y) = \mathcal{L}_{\text{xent}} \left( \left( \beta F(x) + \frac{1-\beta}{K} \sum_{k=1}^K F(\tilde{x}_k) \right), y \right) \quad (18)$$

where  $0 \leq \beta < 1$  is the interpolation coefficient between  $F(x)$  and  $\frac{1}{K} \sum_{k=1}^K F(\tilde{x}_k)$ .

### 4.3 Front-door Adjustment via Fourier-based Style Transfer

Our proposed method for front-door adjustment can seamlessly generalise to other style transfer methods. In this paper, we also consider the *Fourier-based Style Transfer* (FST) used in [29, 58]. This style transfer method applies the discrete Fourier transform to decompose an image into its phase and amplitude, that are considered as content and style, respectively. Unlike NST, FST does not require a training phase. However, its decomposed styles may not as diverse as those learnt from NST.

The Fourier transformation  $\mathcal{F}$  of an image  $x$  can be written  $\mathcal{F}(x) = \mathcal{A}(x) \times e^{-j \times \mathcal{P}(x)}$ , where  $\mathcal{A}(x)$  and  $\mathcal{P}(x)$  denote the amplitude and phase of  $x$ , respectively. Following [58], we use the “amplitude mix” strategy to produce a stylised image  $\hat{x}$  from a content image  $x$  and a style image  $x'$  as follows:

$$\hat{x} = \mathcal{F}^{-1} \left( ((1-\lambda)\mathcal{A}(x) + \lambda\mathcal{A}(x')) \times e^{-j \times \mathcal{P}(x)} \right) \quad (19)$$

where  $\lambda \sim U(0, \eta)$  and  $0 \leq \eta \leq 1$  is a hyper-parameter controlling the maximum style mixing rate.

We name this version as FAFT (**F**ront-door **A**djustment via **F**ourier-based **S**tyl **T**ransfer). We train the classifier  $F$  using the same loss function as in Eq. (18) but with  $\tilde{x}_k$  being replaced by  $\hat{x}_k$  which is given below:

$$\mathcal{L}_{\text{FAFT}}(x, y) = \mathcal{L}_{\text{xent}} \left( \left( \beta F(x) + \frac{1-\beta}{K} \sum_{k=1}^K F(\hat{x}_k) \right), y \right) \quad (20)$$

Since different style transfer approaches capture different styles in the input, one can combine NST and FST together to exploit the strengths of both methods. This results in a more general manner namely FAGT (*F*ront-door *A*djustment via *G*eneral *T*ransfer), where the classification network  $F$  is optimised by the following loss function:

$$\mathcal{L}_{\text{FAGT}}(x, y) = \mathcal{L}_{\text{xent}} \left( \left( \beta F(x) + \frac{1-\beta}{2K} \sum_{k=1}^K [F(\tilde{x}_k) + F(\hat{x}_k)] \right), y \right) \quad (21)$$

### 4.4 Inference by the Causal Dependence

We use the causal dependence  $P(Y|do(X))$  not only for training but also for the inference phase. The association dependence  $P(Y|X)$  could bring spuriousness into predictions, even if the model is trained with the causal objective. In both phases, for all methods, we sample  $K = 3$  training samples from different domains to compute  $P(Y|do(X))$ . We empirically show the effectiveness of using  $P(Y|do(X))$  over  $P(Y|X)$  in both the two phases in Section 5, where the method with causality in both phases clearly outperforms the others. It is worth noting that for every single image  $x$ , we do not

use its neighbors in the representation space as a substitution for either  $\tilde{x}$  or  $\hat{x}$ , since the specific semantics of  $x$  in these samples would not suffice to infer  $P(Y|do(X = x))$ .

## 5 EXPERIMENTS

### 5.1 Datasets

Following previous works [29, 31, 69], we evaluate our proposed methods on three standard OOD generalisation benchmark datasets described below.

**PACS** [24] consists of 9991 images from 4 domains namely Photo ( $P$ ), Art-painting ( $A$ ), Cartoon ( $C$ ), Sketch ( $S$ ). These domains have largely different styles, making this dataset challenging for OOD generalisation. There are 7 classes in each domain. We use the training-validation-test split in [24] for fair comparison.

**Office-Home** [52] contains 15,500 images of office and home objects divided into 65 categories. The images are from 4 domains: Art ( $A$ ), Clipart ( $C$ ), Product ( $P$ ), and Real-world ( $R$ ). We use the training-validation-test split in [71].

**Digits-DG** [68] is comprised of 4 digit domains namely MNIST [21] ( $MN$ ), MNIST-M [10] ( $MM$ ), SVHN [38] ( $SV$ ) and SYN [10] ( $SY$ ) with 10 digit classes (0-9) in each domain. These domains are very different in font style, stroke colour, and background. We follow [68, 70] to select 600 images of each class from each domain, where 80% and 20% of the selected data are used for training and validation respectively.

All images have the size of  $224 \times 224$  for PACS and Office-Home, and  $32 \times 32$  for Digits-DG.

### 5.2 Experimental Setting

We use the leave-one-domain-out strategy [24, 71] for evaluation: a model is tested on an unseen domain after training on all the remaining ones.

**Classifier details:** Following [27, 58, 71], we use pre-trained ResNet-18 [6, 12] backbone for PACS, Office-Home, and a small convolutional network [68] trained from scratch for Digits-DG. For all datasets, we train the network  $F$  for 50 epochs using an SGD optimiser with momentum 0.9, weight decay  $5 \times 10^{-4}$ , batch sizes 64 for Digits-DG and 32 for PACS and Office-Home. For Digits-DG, the initial learning rate is 0.03 and decayed by 0.1 after every 20 epochs, while those for PACS and Office-Home are initialised at 0.001 and follow the cosine annealing schedule. We deploy the standard augmentation protocol in [27, 71], where only random translation is used for Digits-DG while random flipping, random translation, color-jittering, and random gray-scaling are used for PACS and Office-Home.

**NST model details:** For each dataset, we fine-tune the decoder of the pre-trained AdaIN NST [15] model for 70 epochs with all hyper-parameters referenced from [15], whereas its encoder is a *fixed* pre-trained VGG-19 [47] from ImageNet. Since NST models do not work well on small-size images, for Digits-DG, we upscale images to the size of  $(224 \times 224)$  before downscaling to  $(32 \times 32)$  for the classifier  $F$ . We also adopt the leave-one-domain-out strategy when training the NST model and then use the corresponding version for classification.

We find the hyper-parameters  $\alpha$  and  $\beta$  of FAST accordingly for each domain based on a grid search algorithm on the validation set,

Methods	PACS					Office-Home					Digits-DG				
	A	C	P	S	Avg.	A	C	P	R	Avg.	MN	MM	SV	SY	Avg.
ERM [51]	77.0	75.9	96.0	69.2	79.5	58.1	48.7	74.0	75.6	64.2	95.8	58.8	61.7	78.6	73.7
DeepAll [68]	77.6	76.8	95.9	69.5	79.9	57.9	52.7	73.5	74.8	64.7	95.8	58.8	61.7	78.6	73.7
Jigen [3]	79.4	75.3	96.0	71.4	80.5	53.0	47.5	71.5	72.8	61.2	96.5	61.4	63.7	74.0	73.9
CCSA [36]	80.5	76.9	93.6	66.8	79.4	59.9	49.9	74.1	75.7	64.9	95.2	58.2	65.5	79.1	74.5
MMD-AAE [25]	75.2	72.7	96.0	64.2	77.0	56.5	47.3	72.1	74.8	62.7	96.5	58.4	65.0	78.4	74.6
CrossGrad [45]	79.8	76.8	96.0	70.2	80.7	58.4	49.4	73.9	75.8	64.4	96.7	61.1	65.3	80.2	75.8
DDAIG [68]	84.2	78.1	95.3	74.7	83.1	59.2	52.3	<u>74.6</u>	<u>76.0</u>	65.5	96.6	64.1	68.6	81.0	77.6
L2A-OT [69]	83.3	78.2	96.2	73.6	82.8	<b>60.6</b>	50.1	<b>74.8</b>	<b>77.0</b>	65.6	96.7	63.9	68.6	83.2	78.1
RSC [16]	83.4	80.3	96.0	80.9	85.2	58.4	47.9	71.6	74.5	63.1	-	-	-	-	-
MixStyle [71]	83.0	78.6	96.3	71.2	82.3	58.7	53.4	74.2	75.9	65.5	96.5	63.5	64.7	81.2	76.5
FACT [58]	85.4	78.4	95.2	79.2	84.6	60.3	54.9	74.5	76.6	66.6	97.9	65.6	72.4	90.3	81.6
FACT <sup>†</sup>	84.8	78.0	95.3	79.1	84.3	57.9	54.9	73.7	75.0	65.4	95.6	63.3	69.0	82.5	77.6
MatchDG [31]	81.3	<u>80.7</u>	96.5	79.7	84.6	-	-	-	-	-	-	-	-	-	-
CICF [27]	80.7	76.9	95.6	74.5	81.9	57.1	52.0	74.1	75.6	64.7	95.8	63.7	65.8	80.7	76.5
CIRL [29]	86.1	80.6	95.9	82.7	86.3	61.5	55.3	75.1	76.6	67.1	96.1	69.8	76.2	87.7	82.5
CIRL <sup>†</sup>	85.9	79.8	95.6	81.4	85.7	58.6	<b>55.4</b>	73.8	75.1	65.7	95.4	<b>65.9</b>	68.9	82.0	78.1
FAST (ours)	<u>86.5</u>	80.7	<u>96.6</u>	81.0	<u>86.2</u>	59.6	54.5	74.1	75.7	<u>66.0</u>	<u>97.9</u>	64.0	<u>70.5</u>	<u>90.0</u>	<u>80.6</u>
FAFT (ours)	86.3	80.3	96.4	80.8	86.0	60.0	53.6	73.9	75.7	65.8	97.8	62.9	68.5	89.6	79.7
FAGT (ours)	<b>87.5</b>	<b>80.9</b>	<b>96.9</b>	<b>81.9</b>	<b>86.8</b>	<u>60.1</u>	<u>55.0</u>	74.5	75.8	<b>66.4</b>	<b>98.3</b>	<u>65.7</u>	<b>70.9</b>	<b>90.4</b>	<b>81.3</b>

**Table 1: Leave-one-domain-out classification accuracies (in %) on PACS, Office-Home, and Digits-DG. In ERM, we simply train the classifier on all domains except the test one. FACT<sup>†</sup> and CIRL<sup>†</sup> denote our rerun of FACT and CIRL respectively using the authors’ official codes following the same settings in the original papers. We use the results from FACT<sup>†</sup> and CIRL<sup>†</sup> for fair comparison with our method. The best and second-best results are highlighted in bold and underlined respectively.**

whereas the hyper-parameters of the FST in FAFT are referenced from [29, 58]. In both the training and inference phases, for each method, we sample  $K = 3$  training samples from *different domains* and compute  $P(Y|\text{do}(X))$  using the same formula in Eqs. 18, 20, and 21. More implementation details are given in the supplementary. We repeat the experiment ten times with different seed values and report the average results.

### 5.3 Experimental Results

In Table 1, we show the domain generalisation results on the three benchmark datasets. The baselines are divided into two groups: non-causality-based methods (from DeepAll [68] to FACT [58]), and causality-based methods (from MatchDG [31] to CIRL [29]).

It is clear that our methods significantly outperform almost all non-causality-based baselines on all datasets, suggesting the advantage of causal inference for OOD generalisation. For example, FAGT achieves about 4.5/0.9% and 1.6/3.3% higher accuracy than MixStyle [71] and RSC [16] respectively on PACS/Office-Home. It is worth noting that MixStyle and RSC are both quite strong baselines. However, they still rely on the superficial statistical dependence  $P(Y|X)$ , instead of our modelling the causal dependence  $P(Y|\text{do}(X))$ . Our methods also improve by about 4% and 2% over L2A-OT [69] and FACT [58] accordingly on PACS. However, FAGT achieves slightly lower accuracies compared to L2A-OT in some domains of Office-Home, while beating it by a large margin of about 5% on the most challenging domain *Clipart*. On Office-Home

and Digits-DG, although FAGT remains competitive with FACT on almost all domains, our performance drops a little in *Real-world* of Office-Home and *SVHN* of Digits-DG. We note that although we try but cannot reproduce the results of FACT reported in their paper. In the source codes of FACT, the authors do not provide the config files for Office-Home and Digits-DG datasets. Thus, we follow the experimental setting and hyper-parameters shown in their paper and rerun their source codes ten times but cannot replicate the reported results. We use the best results of FACT among our reruns for fairness and report as FACT<sup>†</sup>. Our methods show superior performance over FACT<sup>†</sup> in all datasets.

It can be observed that FAST surpasses MatchDG [31], a quite state-of-the-art (SOTA) causality-based method that aims to learn domain-invariant representation, by about 5.0% and 1.3% in *Art-Painting* and *Sketch* on PACS respectively. We compare our methods with CICF [27], a recent method that interprets the causal front-door formula (Eq. 9) via the meta-learning perspective. In some challenging domains (e.g., *Clipart* of Office-Home or *SYN* of Digits-DG) where testing images appear with diverse domain-specific confounders such as colourful backgrounds, our methods significantly outperform CICF. This suggests that the style-based information of our style transfer algorithms is more crucial to mitigating the spurious correlations of confounders than the gradient-based meta-learning information of CICF. On PACS, FAGT beats CIRL in terms of the average accuracy over all domains. It is worth noting that

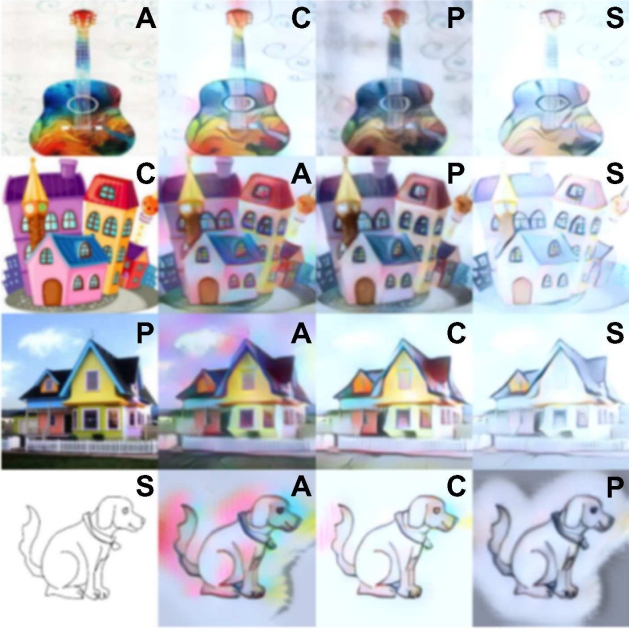


Figure 3: Visualisation of how unseen novel domains can be translated back to the learnt ones without hurting the main content by FAST on PACS. Each testing image is plotted in the first column, where the remaining columns visualise its translated version in the trained domains. Domain labels are noted at the upper right corner of each image.

CIRL is a current SOTA method in OOD generalisation and an improvement of 1.4% over it in *Art-painting* of PACS is considerable. However, on Office-Home and Digits-DG, CIRL outperforms our methods in some domains (e.g., *Art* of Office-Home, *MNIST-M* and *SVHN* of Digits-DG). The improvement of CIRL is owing to their Factorisation and Adversarial Mask modules, making the method more complicated than ours. Besides the causal intervention, CIRL also makes use of an adversarial mask that significantly improves its performance. From Table 5 in the CIRL paper, it is clear that if the adversarial mask is removed (Variant 3), the performance of CIRL on PACS will drop by nearly 1% to 85.43 and is much worse than our proposed method. By contrast, our methods learn a plain classifier with only the maximum interventional likelihood objective and can achieve more than 86% average accuracy on PACS. Similar to FACT, we try but cannot reproduce the results of CIRL. We rerun their source codes ten times, and report the best results among our reruns as CIRL<sup>†</sup> for fairness. Compared to CIRL<sup>†</sup>, FAGT surpasses it by 1.1%, 0.7%, and 3.2% on PACS, Office-Home, and Digits-DG respectively.

*Discussion about why our method works.* We argue three main reasons behind the success of our methods in OOD generalisation. Owing to the AdaIn NST model, our methods could map any novel domain back to the learnt ones without hurting the content of images, which is beneficial for computing  $P(Y|do(X))$ . We visually justify this point in Fig. 3.

Causal Dependence		PACS				
Training	Inference	A	C	P	S	Avg.
-	-	84.8	78.8	96.2	79.1	84.8
✓	-	85.1	79.1	96.4	79.0	84.9
✓	✓	87.5	80.9	96.9	81.9	86.8

Table 2: The performance of our FAGT method with and without using the causal dependence in the training and inference phases. All methods are conducted on the same experimental setting, the method without causality in both the phases uses augmented samples  $\tilde{x}$  or  $\hat{x}$  for a fair comparison. Overall, the method with causality in both phases clearly outperforms the others.

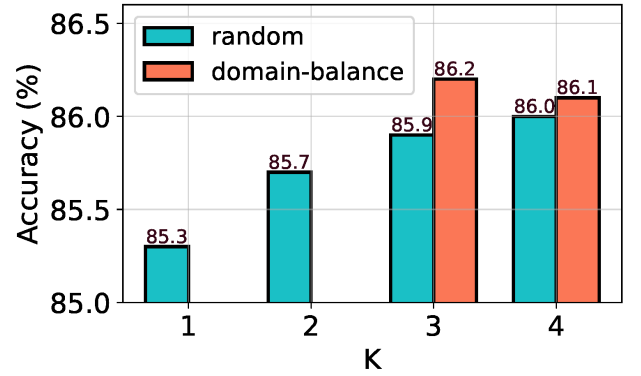


Figure 4: Accuracies (in %) of FAST on PACS with different numbers of style images  $K$ . “random” and “domain-balance” denote two sampling strategies of style images.

On the other hand, our great performance would be largely contributed by modelling the causal dependence via front-door adjustment, which we show to be invariant across domains in Sections 3, 4. In Table 2, we show the effectiveness of using  $P(Y|do(X))$  over  $P(Y|X)$  in both the training and inference phases, where the method with causality in both phases clearly outperforms the others. Many recent state-of-the-art causality-based methods in OOD generalisation enforce regularisation with different data transformations on the learnt feature to achieve the domain-invariant feature [29, 31, 55]. Although achieving promising results, the regularisation objectives may have gradient conflicts with other learning objectives of the model, leading to inferior performance in some cases [4].

Asides, our front-door adjustment solution is orthogonal and more flexible, since various stylised images can be taken into account to eliminate spurious correlations of confounders, favouring the causal dependence  $P(Y|do(X))$ . This is validated by the superior performance of FAGT across all the experimented datasets. Further, our estimation of the causal front-door formula via style transfer algorithms in Eq. 9 is reasonable and general, enabling various stylised images in both FAST and FAFT to be taken into account for mitigating the negative correlations of confounders.

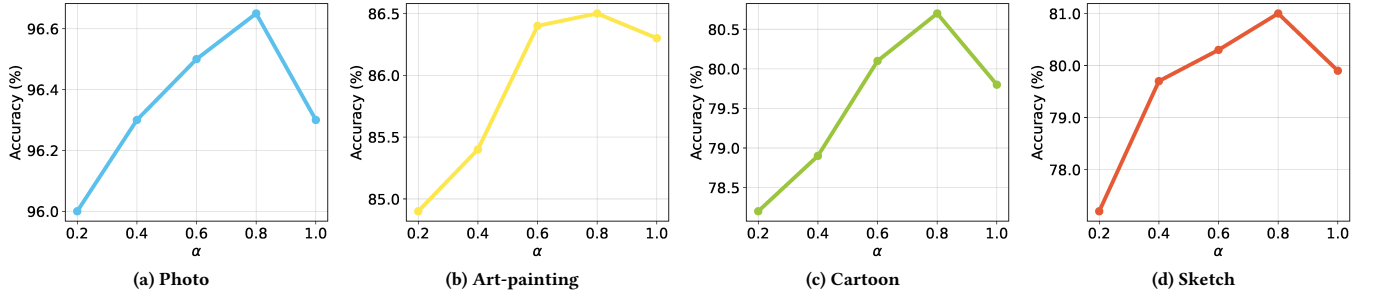


Figure 5: The performance of FAST on the test domains of PACS with different values of the style mixing coefficient  $\alpha$ .

## 5.4 Ablation Studies



Figure 6: Visualisation of stylised images with different values of  $\alpha$ . The first and last columns contain content and style images respectively. The middle columns contain stylised images w.r.t.  $\alpha$  being 0.2, 0.4, 0.6, 0.8, and 1.0 respectively.

**Number of style images.** We study the impact of the number of style images  $K$  (Eq. 18) on the performance of FAST. In Fig. 4, we show the average results of FAST on PACS with  $K$  varying from 1 to 4. We see that i) increasing the number of style images often lead to better results when these images are sampled randomly from the training data, and ii) we can improve the results further by ensuring a balance in the number of sampled style images across domains.

**Trade-off between content and style.** In Fig. 5, we show the results of FAST on each test domain of PACS with the style mixing coefficient  $\alpha$  (Eq. 13) taking different values in  $\{0.2, 0.4, 0.6, 0.8, 1.0\}$ . It is clear that FAST achieves higher accuracies on all the test domains when  $\alpha$  becomes larger (up to 0.8), or equivalently, when  $\tilde{x}$  more likely contains the style of  $x'$ . This empirically justifies the reasonability of using style transfer to model front-door adjustment. However, if  $\alpha$  is too large (e.g.,  $\alpha = 1.0$ ), the performance of FAST drops. This is because too large  $\alpha$  leads to the loss of content information in the stylised images as shown in Fig. 6.

## 6 CONCLUSION

This paper studies the problem of Out-of-distribution (OOD) generalisation from the causality perspective. We show that statistical learning methods are ineffective for OOD generalisation due to spurious correlations from domain-specific confounders into model training, resulting in instability to domain shifting. The most commonly used causal inference method, back-door adjustment, is unfeasible since the method requires the observation of confounders, which is impractical in the setting. We address the issue via front-door adjustment where features essential to label prediction are considered the mediator variable. It is not trivial to interpret the front-door formula, and we propose novel methods that estimate it based on many style transfer models. We evaluated our methods on several benchmark datasets. Experimental results show the superiority of our method over existing baselines in OOD generalisation.

## REFERENCES

- [1] Martin Arjovsky, Léon Bottou, Ishaan Gulrajani, and David Lopez-Paz. 2019. Invariant risk minimization. *arXiv preprint arXiv:1907.02893* (2019).
- [2] Michael Baiocchi, Jing Cheng, and Dylan S Small. 2014. Instrumental variable methods for causal inference. *Statistics in medicine* 33, 13 (2014), 2297–2340.
- [3] Fabio M. Carlucci, Antonio D’Innocente, Silvia Bucci, Barbara Caputo, and Tatiana Tommasi. 2019. Domain Generalization by Solving Jigsaw Puzzles. In *CVPR*.
- [4] Yongqiang Chen, Kaiwen Zhou, Yatao Bian, Binghui Xie, Bingzhe Wu, Yonggang Zhang, MA KAILI, Han Yang, Peilin Zhao, Bo Han, et al. 2023. Pareto invariant risk minimization: Towards mitigating the optimization dilemma in out-of-distribution generalization. In *ICLR*.
- [5] Ekin D. Cubuk, Barret Zoph, Dandelion ManÃ©, Vijay Vasudevan, and Quoc V. Le. 2019. AutoAugment: Learning Augmentation Strategies From Data. In *CVPR*. 113–123.
- [6] Jia Deng, Wei Dong, Richard Socher, Li-Jia Li, Kai Li, and Li Fei-Fei. 2009. ImageNet: A large-scale hierarchical image database. In *CVPR*. 248–255.
- [7] Xiang Deng and Zhongfei Zhang. 2022. Deep Causal Metric Learning. In *ICML*. PMLR, 4993–5006.
- [8] Qi Dou, Daniel Coelho de Castro, Konstantinos Kamnitsas, and Ben Glocker. 2019. Domain generalization via model-agnostic learning of semantic features. *NeurIPS* 32 (2019).
- [9] Bao Duong and Thin Nguyen. 2022. Bivariate causal discovery via conditional divergence. In *CLeaR*. PMLR, 236–252.
- [10] Yaroslav Ganin and Victor Lempitsky. 2015. Unsupervised domain adaptation by backpropagation. In *ICML*. PMLR, 1180–1189.
- [11] Madelyn Glymour, Judea Pearl, and Nicholas P Jewell. 2016. *Causal inference in statistics: A primer*. John Wiley & Sons.
- [12] Kaiming He, Xiangyu Zhang, Shaoqing Ren, and Jian Sun. 2016. Deep residual learning for image recognition. In *CVPR*. 770–778.
- [13] Dan Hendrycks, Steven Basart, Norman Mu, Saurav Kadavath, Frank Wang, Evan Dorundo, Rahul Desai, Tyler Zhu, Samyak Parajuli, Mike Guo, et al. 2021. The many faces of robustness: A critical analysis of out-of-distribution generalization. In *ICCV*. 8340–8349.



- [14] Jianqiang Huang, Yu Qin, Jiaxin Qi, Qianru Sun, and Hanwang Zhang. 2022. Deconfounded visual grounding. In *AAAI*. 998–1006.
- [15] Xun Huang and Serge Belongie. 2017. Arbitrary style transfer in real-time with adaptive instance normalization. In *CVPR*. 1501–1510.
- [16] Zeyi Huang, Haohan Wang, Eric P Xing, and Dong Huang. 2020. Self-challenging improves cross-domain generalization. In *ECCV*. Springer, 124–140.
- [17] Zhuo Huang, Xiaobo Xia, Li Shen, Bo Han, Mingming Gong, Chen Gong, and Tongliang Liu. 2023. Harnessing Out-Of-Distribution Examples via Augmenting Content and Style. In *ICLR*.
- [18] Aapo Hyvarinen, Hiroaki Sasaki, and Richard Turner. 2019. Nonlinear ICA using auxiliary variables and generalized contrastive learning. In *AISTATS*. PMLR, 859–868.
- [19] Yibo Jiang and Victor Veitch. 2022. Invariant and Transportable Representations for Anti-Causal Domain Shifts. In *NeurIPS*, Alice H. Oh, Alekh Agarwal, Danielle Belgrave, and Kyunghyun Cho (Eds.).
- [20] Yongcheng Jing, Yezhou Yang, Zunlei Feng, Jingwen Ye, Yizhou Yu, and Mingli Song. 2019. Neural style transfer: A review. *TVCG* 26, 11 (2019), 3365–3385.
- [21] Yann LeCun, Léon Bottou, Yoshua Bengio, and Patrick Haffner. 1998. Gradient-based learning applied to document recognition. *Proc. IEEE* 86, 11 (1998), 2278–2324.
- [22] Da Li, Yongxin Yang, Yi-Zhe Song, and Timothy Hospedales. 2018. Learning to generalize: Meta-learning for domain generalization. In *AAAI*.
- [23] Da Li, Yongxin Yang, Yi-Zhe Song, and Timothy Hospedales. 2020. Sequential learning for domain generalization. In *ECCV*. Springer, 603–619.
- [24] Da Li, Yongxin Yang, Yi-Zhe Song, and Timothy M Hospedales. 2017. Deeper, broader and artier domain generalization. In *ICCV*. 5542–5550.
- [25] Haoliang Li, Sinno Jialin Pan, Shiqi Wang, and Alex C. Kot. 2018. Domain Generalization With Adversarial Feature Learning. In *CVPR*.
- [26] Lei Li, Veronika A Zimmer, Wangbin Ding, Fuping Wu, Liqin Huang, Julia A Schnabel, and Xiahai Zhuang. 2021. Random style transfer based domain generalization networks integrating shape and spatial information. In *Statistical Atlases and Computational Models of the Heart. M&Ms and EMIDEC Challenges: 11th International Workshop, STACOM 2020, Held in Conjunction with MICCAI 2020, Lima, Peru, October 4, 2020, Revised Selected Papers 11*. Springer, 208–218.
- [27] Xin Li, Zhizheng Zhang, Guoqiang Wei, Cuiling Lan, Wenjun Zeng, Xin Jin, and Zhibo Chen. 2021. Confounder Identification-free Causal Visual Feature Learning. *arXiv preprint arXiv:2111.13420* (2021).
- [28] Ya Li, Xinmei Tian, Mingming Gong, Yajing Liu, Tongliang Liu, Kun Zhang, and Dacheng Tao. 2018. Deep domain generalization via conditional invariant adversarial networks. In *ECCV*. 624–639.
- [29] Fangrui Lv, Jian Liang, Shuang Li, Bin Zang, Chi Harold Liu, Ziteng Wang, and Di Liu. 2022. Causality Inspired Representation Learning for Domain Generalization. In *CVPR*. 8046–8056.
- [30] Sara Magliacane, Thijs Van Ommen, Tom Claassen, Stephan Bongers, Philip Versteeg, and Joris M Mooij. 2018. Domain adaptation by using causal inference to predict invariant conditional distributions. *NeurIPS* 31 (2018).
- [31] Divyat Mahajan, Shruti Tople, and Amit Sharma. 2021. Domain generalization using causal matching. In *ICML*. PMLR, 7313–7324.
- [32] Chengzhi Mao, Kevin Xia, James Wang, Hao Wang, Junfeng Yang, Elias Bareinboim, and Carl Vondrick. 2022. Causal Transportability for Visual Recognition. In *CVPR*. 7521–7531.
- [33] Qiaowei Miao, Junkun Yuan, and Kun Kuang. 2022. Domain Generalization via Contrastive Causal Learning. *arXiv preprint arXiv:2210.02655* (2022).
- [34] Wang Miao, Zhi Geng, and Eric J Tchetgen Tchetgen. 2018. Identifying causal effects with proxy variables of an unmeasured confounder. *Biometrika* 105, 4 (2018), 987–993.
- [35] Jovana Mitrovic, Brian McWilliams, Jacob C Walker, Lars Holger Buesing, and Charles Blundell. 2021. Representation Learning via Invariant Causal Mechanisms. In *ICLR*. <https://openreview.net/forum?id=9p2ekP904Rs>
- [36] Saeid Motiian, Marco Piccirilli, Donald A Adjeroh, and Gianfranco Doretto. 2017. Unified deep supervised domain adaptation and generalization. In *ICCV*. 5715–5725.
- [37] Krikamol Muandet, David Balduzzi, and Bernhard Schölkopf. 2013. Domain generalization via invariant feature representation. In *ICML*. PMLR, 10–18.
- [38] Yuval Netzer, Tao Wang, Adam Coates, Alessandro Bissacco, Bo Wu, and Andrew Y Ng. 2011. Reading digits in natural images with unsupervised feature learning. *NeurIPS* (2011).
- [39] Judea Pearl. 1995. Causal diagrams for empirical research. *Biometrika* 82, 4 (1995), 669–688.
- [40] Xingchao Peng and Kate Saenko. 2018. Synthetic to real adaptation with generative correlation alignment networks. In *WACV*. IEEE, 1982–1991.
- [41] Jonas Peters, Dominik Janzing, and Bernhard Schölkopf. 2017. *Elements of causal inference: foundations and learning algorithms*. The MIT Press.
- [42] Mateo Rojas-Carulla, Bernhard Schölkopf, Richard Turner, and Jonas Peters. 2018. Invariant models for causal transfer learning. *JMLR* 19, 1 (2018), 1309–1342.
- [43] Bernhard Schölkopf, Francesco Locatello, Stefan Bauer, Nan Rosemary Ke, Nal Kalchbrenner, Anirudh Goyal, and Yoshua Bengio. 2021. Toward Causal Representation Learning. *Proc. IEEE* 109, 5 (2021), 612–634.
- [44] Bernhard Schölkopf and Julius von Kügelgen. 2022. From statistical to causal learning. *arXiv preprint arXiv:2204.00607* (2022).
- [45] Shiv Shankar, Vihari Piratla, Soumen Chakrabarti, Siddhartha Chaudhuri, Preethi Jyothi, and Sunita Sarawagi. 2018. Generalizing Across Domains via Cross-Gradient Training. In *ICLR*. <https://openreview.net/forum?id=r1Dx7fbCW>
- [46] Zheyang Shen, Jiashuo Liu, Yue He, Xingxuan Zhang, Renzhe Xu, Han Yu, and Peng Cui. 2021. Towards out-of-distribution generalization: A survey. *arXiv preprint arXiv:2108.13624* (2021).
- [47] Karen Simonyan and Andrew Zisserman. 2014. Very deep convolutional networks for large-scale image recognition. *arXiv preprint arXiv:1409.1556* (2014).
- [48] Xinwei Sun, Botong Wu, Xiangyu Zheng, Chang Liu, Wei Chen, Tao Qin, and Tie-Yan Liu. 2021. Recovering latent causal factor for generalization to distributional shifts. *NeurIPS* 34 (2021), 16846–16859.
- [49] Kaihua Tang, Mingyuan Tao, and Hanwang Zhang. 2021. Adversarial visual robustness by causal intervention. *arXiv preprint arXiv:2106.09534* (2021).
- [50] Takeshi Teshima, Issei Sato, and Masashi Sugiyama. 2020. Few-shot domain adaptation by causal mechanism transfer. In *ICML*. PMLR, 9458–9469.
- [51] Vladimir N. Vapnik. 1998. *Statistical Learning Theory*. Wiley-Interscience.
- [52] Hemant Venkateswara, Jose Eusebio, Shayok Chakraborty, and Sethuraman Panchanathan. 2017. Deep hashing network for unsupervised domain adaptation. In *CVPR*. 5018–5027.
- [53] Julius Von Kügelgen, Yash Sharma, Luigi Gresele, Wieland Brendel, Bernhard Schölkopf, Michel Besserve, and Francesco Locatello. 2021. Self-supervised learning with data augmentations provably isolates content from style. *NeurIPS* 34 (2021), 16451–16467.
- [54] Pengfei Wang, Zhaoxiang Zhang, Zhen Lei, and Lei Zhang. 2023. Sharpness-Aware Gradient Matching for Domain Generalization. In *CVPR*. 3769–3778.
- [55] Ruoyu Wang, Mingyang Yi, Zhitang Chen, and Shengyu Zhu. 2022. Out-of-distribution Generalization with Causal Invariant Transformations. In *CVPR*. 375–385.
- [56] Tan Wang, Jianqiang Huang, Hanwang Zhang, and Qianru Sun. 2020. Visual commonsense r-cnn. In *CVPR*. 10760–10770.
- [57] Zehao Xiao, Jiayi Shen, Xiantong Zhen, Ling Shao, and Cees Snoek. 2021. A bit more bayesian: Domain-invariant learning with uncertainty. In *ICML*. PMLR, 11351–11361.
- [58] Qinwei Xu, Ruipeng Zhang, Ya Zhang, Yanfeng Wang, and Qi Tian. 2021. A fourier-based framework for domain generalization. In *CVPR*.
- [59] Xu Yang, Hanwang Zhang, and Jianfei Cai. 2021. Deconfounded image captioning: A causal retrospect. *TPAMI* (2021).
- [60] Xu Yang, Hanwang Zhang, Guojun Qi, and Jianfei Cai. 2021. Causal attention for vision-language tasks. In *CVPR*. 9847–9857.
- [61] Liuyi Yao, Zhixuan Chu, Sheng Li, Yaliang Li, Jing Gao, and Aidong Zhang. 2021. A survey on causal inference. *TKDD* 15, 5 (2021), 1–46.
- [62] Zhongqi Yue, Qianru Sun, Xian-Sheng Hua, and Hanwang Zhang. 2021. Transporting causal mechanisms for unsupervised domain adaptation. In *ICCV*. 8599–8608.
- [63] Dong Zhang, Hanwang Zhang, Jinhui Tang, Xian-Sheng Hua, and Qianru Sun. 2020. Causal intervention for weakly-supervised semantic segmentation. *NeurIPS* 33 (2020), 655–666.
- [64] Kun Zhang, Bernhard Schölkopf, Krikamol Muandet, and Zhikun Wang. 2013. Domain adaptation under target and conditional shift. In *ICML*. PMLR, 819–827.
- [65] Yabin Zhang, Minghan Li, Ruihuang Li, Kui Jia, and Lei Zhang. 2022. Exact feature distribution matching for arbitrary style transfer and domain generalization. In *CVPR*. 8035–8045.
- [66] Yuyang Zhao, Zhun Zhong, Fengxiang Yang, Zhiming Luo, Yaojin Lin, Shaozi Li, and Nicu Sebe. 2021. Learning to generalize unseen domains via memory-based multi-source meta-learning for person re-identification. In *CVPR*. 6277–6286.
- [67] Kaiyang Zhou, Ziwei Liu, Yu Qiao, Tao Xiang, and Chen Change Loy. 2022. Domain generalization: A survey. *TPAMI* (2022).
- [68] Kaiyang Zhou, Yongxin Yang, Timothy Hospedales, and Tao Xiang. 2020. Deep domain-adversarial image generation for domain generalisation. In *AAAI*. 13025–13032.
- [69] Kaiyang Zhou, Yongxin Yang, Timothy Hospedales, and Tao Xiang. 2020. Learning to generate novel domains for domain generalization. In *ECCV*. Springer, 561–578.
- [70] Kaiyang Zhou, Yongxin Yang, Yu Qiao, and Tao Xiang. 2021. Domain adaptive ensemble learning. *TIP* 30 (2021), 8008–8018.
- [71] Kaiyang Zhou, Yongxin Yang, Yu Qiao, and Tao Xiang. 2021. Domain Generalization with MixStyle. In *ICLR*.

In this supplementary material, we first provide a detailed derivation of the front-door formula used in our method, and a proof sketch on the fulfillment of our proposed algorithms with the front-door criterion in Section A. In Section B, we give a complete derivation of the Maximum Interventional Log-likelihood in our formulation of OOD generalisation under the causal perspective. We show our experimental results with ResNet-50 [12] on PACS and Office-Home in Section C. A comprehensive description of experimental setup including parameter settings is given in Section D. We make more ablation studies and discussion about our method in Section E. Finally, we visualise several stylised images produced by our algorithms in Section F.

## A DETAILS ON FRONT-DOOR ADJUSTMENT IN OOD GENERALISATION

### A.1 Derivation of Front-door Adjustment

In this section, we provide a mathematical derivation for the front-door adjustment of  $P(Y|do(x))$  in the main text. Recalling that for front-door adjustment, we use a mediator variable  $Z$  between  $X$  and  $Y$  which satisfies the following conditions: (i) All directed paths from  $X$  to  $Y$  flow through  $Z$ . (ii)  $X$  blocks all back-door paths from  $Z$  to  $Y$ . (iii) There are no unblocked back-door paths from  $X$  to  $Z$ . Then, we can identify  $P(Y|do(x))$  as below:

$$P(Y|do(x)) = \sum_z p(z|do(x))P(Y|z, do(x)) \quad (22)$$

$$= \sum_z p(z|x)P(Y|do(z), do(x)) \quad (23)$$

$$= \sum_z p(z|x)P(Y|do(z)) \quad (24)$$

$$= \sum_z p(z|x) \left( \sum_{x'} p(x')P(Y|z, x') \right) \quad (25)$$

$$= \mathbb{E}_{p(z|x)} \mathbb{E}_{p(x')} [P(Y|z, x')] \quad (26)$$

Eq. (22) follows the standard probabilistic rules to incorporate  $z$  into the formula of  $P(Y|do(x))$ . In Eq. (23),  $p(z|x) = p(z|do(x))$  due to condition (iii);  $P(Y|z, do(x)) = P(Y|do(z), do(x))$  due to condition (ii). In Eq. (24),  $P(Y|do(z), do(x)) = P(Y|do(z))$  due to condition (i). In Eq. (25),  $\sum_{x'} p(x')P(Y|z, x')$  is just the back-door adjustment of  $P(Y|do(z))$  with condition (ii) satisfied. Eq. (26) is a rewriting of Eq. (25) using the expectation notation.

### A.2 Satisfaction of the front-door criterion

In this section, we provide a proof sketch that  $Z$  as semantic features in  $X$  will satisfy the front-door criterion.

**Claims:** Let  $Z$  is a variable that captures all and only the semantics in  $X$ . Then,  $Z$  will satisfy the front-door criterion.

**Justification:**

- *All the directed paths  $X \rightarrow Y$  are intercepted by  $Z$ .* Intuitively, the label variable  $Y$  is defined from  $X$  only by its semantic features that are *always* predictive of  $Y$ . In reality, the annotators might only use these features to define  $Y$  from observing  $X$  (e.g., by noticing main objects in  $X$ ). In our methods,  $Z$  learnt by FAST and FAFT fulfills the above condition. In FAFT,  $Z$  is regarded as the phase component of

the Fourier Transformation of  $X$ , which has been shown to preserve most of the high-level semantics such as edges or contours of objects [58]. According to [15], once the AdaIN NST model has been trained well, its output  $\hat{z}$  captures and preserves the semantics of  $x$ , which are transferred from  $z$ .

- *No unblocked back-door paths from  $X$  to  $Z$ .* This requirement suggests that we could estimate the causal relationship ( $X \rightarrow Z$ ) by observing training images, i.e.,  $P(Z|do(X)) = P(Z|X)$ . In both FAST and FAFT,  $Z$  is a *mapping from  $X$*  that sufficiently extract only semantic features in  $X$  via the encoder  $E$  of the AdaIN NST model and the Fourier Transformation respectively. It is worth noting that the trivial identity mapping should not be appropriate, because it may map nuisance confounding features into  $Z$ . Overall,  $Z$  is defined only from  $X$ , thus  $Z$  has no causal parent other than  $X$  in  $\mathcal{G}$  and there will be no confounder between  $X$  and  $Z$ . Therefore, we have  $P(Z|X, d, u) = P(Z|X)$  for any confounder  $d, u$  and we can derive  $P(Z|do(X))$  as follows:

$$P(Z|do(X)) = \sum_{d,u} P(d, u)P(Z|d, u, X) \quad (27)$$

$$= \sum_{d,u} P(d, u)P(Z|X) \quad (28)$$

$$= P(Z|X) \quad (29)$$

- *$X$  blocks all back-door paths from  $Z$  to  $Y$ .* Given no confounder that connects to  $Z$ , according to the causal graph shown in Fig. 2(b), we can see that there is only one back-door path from  $Z$  to  $Y$ , i.e.,  $Z \leftarrow X \leftarrow (D, U) \rightarrow Y$ . Therefore, we can condition on  $X$  to block all the back-door paths from  $Z$  to  $Y$ .

Finally, we conclude that the variable  $Z$  as all and only semantic features in  $X$  in our method will satisfy the front-door criterion.

## B DERIVATION OF THE MAXIMUM INTERVENTIONAL LOG-LIKELIHOOD

In this section, we provide a detailed mathematical derivation of the Maximum Interventional Log-likelihood (MIL) criterion presented in Section 3.1. Assuming there is a causal (interventional) distribution  $P(Y|do(X))$  and a training set  $\mathcal{D}$  contains  $n$  samples  $\{(x_i, y_i)\}_{i=1}^n$ . We consider  $do(x_1), \dots, do(x_n)$  as  $n$  interventions on  $X$  which lead to  $n$  random potential outcomes  $Y_1, \dots, Y_n$ . The joint probability of these potential outcomes is  $P(Y_1, \dots, Y_n|do(x_1), \dots, do(x_n))$ . Since modelling this distribution is difficult and impractical, we factorise it as follows:

$$\begin{aligned} &P(Y_1, \dots, Y_n|do(x_1), \dots, do(x_n)) \\ &= \prod_{i=1}^n P(Y_i|do(x_1), \dots, do(x_n)) \end{aligned} \quad (30)$$

$$= \prod_{i=1}^n P(Y_i|do(x_i)) \quad (31)$$

Eq. (30) depends on a condition saying that the outcome of a particular item  $i$  is independent of the outcomes of other items once the interventions of all the items are provided. This condition generally satisfies since we usually consider causal graphs containing no loop on  $Y$ . Eq. (31) is based on the “no-interference” assumption [61]



Methods	PACS					Office-Home				
	A	C	P	S	Avg.	A	C	P	R	Avg.
ERM [51]	84.7	80.8	97.2	79.3	85.5	63.1	51.9	77.2	78.1	67.6
MMD-AAE [25]	86.1	79.4	96.6	76.5	84.7	60.4	53.3	74.3	77.4	66.4
RSC [16]	85.4	79.7	97.6	78.2	85.2	60.7	51.4	74.8	75.1	65.5
MixStyle [71]	86.8	79.0	96.6	78.5	85.2	-	-	-	-	-
CCM [33]	-	-	-	-	87.0	-	-	-	-	69.7
SAGM [54]	87.4	80.2	<b>98.0</b>	80.8	86.6	65.4	57.0	<b>78.0</b>	<b>80.0</b>	70.1
FACT [58]	89.6	81.8	96.8	84.5	88.2	-	-	-	-	-
MatchDG [31]	85.6	82.1	97.9	78.8	86.1	-	-	-	-	-
CICF <sup>†</sup> [27]	89.7	82.2	97.9	86.2	89.0	63.1	<u>59.4</u>	77.4	78.1	69.5
CIRL [29]	<b>90.7</b>	<b>84.3</b>	97.8	<b>87.7</b>	<b>90.1</b>	-	-	-	-	-
FAST (ours)	89.2	83.4	97.3	82.5	88.1	65.7	59.4	77.7	78.7	70.4
FAFT (ours)	89.4	83.3	97.5	82.3	88.1	<u>65.9</u>	58.3	<u>77.8</u>	78.9	70.2
FAGT (ours)	<u>90.4</u>	<u>83.8</u>	97.7	83.1	88.8	<b>66.3</b>	<b>59.5</b>	77.6	<u>79.0</u>	<b>70.6</b>

**Table 3: Leave-one-domain-out classification accuracies (in %) on PACS, Office-Home with ResNet-50. In ERM, we simply train the classifier on all domains except the test one. CICF<sup>†</sup> as reported in [27] is the original CICF method with AutoAugment [5]. The best and second-best results are highlighted in bold and underlined respectively.**

Domains	FAST	FAFT	FAGT
	$\alpha, \beta$	$\beta$	$\alpha, \beta$
All	[0.6, 0.8], [0.25, 0.45]	[0.25, 0.45]	[0.6, 0.8], [0.15, 0.3]
A, P, R	[0.4, 0.6], [0.35, 0.55]	[0.35, 0.55]	[0.4, 0.6], [0.15, 0.3]
C	[0.5, 0.7], [0.35, 0.55]	[0.35, 0.55]	[0.5, 0.7], [0.15, 0.3]
All	[0.4, 0.6], [0.35, 0.55]	[0.35, 0.55]	[0.4, 0.6], [0.15, 0.3]

**Table 4: Details on hyper-parameters of our models (values of  $\alpha$  in Eq. (13) and  $\beta$  in Eqs. 18, 20, and 21) in each domain on PACS (first row), Office-Home (second row), and Digits-DG (third row). “All” stands for all domains.**

saying that the potential outcome  $Y_i$  of an item  $i$  does not depend on the interventions  $\text{do}(x_j)$  of other items  $j \neq i$ . The factorised distribution in Eq. (31) allows us to model  $P(Y|\text{do}(X))$ .

Next, we want to know the most probable potential outcome under the intervention  $\text{do}(x_i)$  given that the outcome  $y_i$  w.r.t. the treatment  $x_i$  was observed. The “consistency” assumption [61] provides us with an answer to this question. It states that the observed outcome  $y_i$  w.r.t. to a treatment  $x_i$  of an item  $i$  is the potential outcome  $Y_i$  under the intervention  $\text{do}(x_i)$ . This means  $Y_i|\text{do}(x_i)$  is likely to be  $y_i$ , and it is reasonable to maximise  $P(Y_i = y_i|\text{do}(x_i))$ .

Therefore, given the “no-interference” and “consistency” assumptions, we can learn a causal model  $P_\theta(Y|\text{do}(X))$  from an observational training set  $\mathcal{D}$  by optimising the following objective:

$$\theta^* = \underset{\theta}{\operatorname{argmax}} \mathbb{E}_{(x,y) \sim \mathcal{D}} [\log P_\theta(Y = y|\text{do}(x))]$$

which we refer to as the *Maximum Interventional Log-likelihood (MIL)*.

## C RESULTS WITH RESNET-50 ON PACS AND OFFICE-HOME

We conducted more experiments on PACS and Office-Home with backbone ResNet-50. All hyper-parameters are the same as those

used with ResNet-18. In Table 3, we show the domain generalisation results on PACS and Office-Home with ResNet-50. The baselines are divided into two groups: non-causality-based methods (from MMD-AAE [25] to FACT [58]), and causality-based methods (from MatchDG [31] to CIRL [29]).

As can be seen from Table 3, our proposed methods outperform non-causality-based methods by a large margin on both datasets, validating the effectiveness of causal inference in OOD generalisation. For example, FAGT achieves 3.6% and 0.6% higher accuracy than MixStyle [71] and FACT [58] respectively on PACS. Among causality-based methods, FAGT remains competitive with CICF<sup>†</sup> [27] although our algorithm does not use as strong augmentation techniques as CICF<sup>†</sup>. On the other hand, FAGT surpasses CICF<sup>†</sup> by a large margin of 1.1% on Office-Home, which demonstrates our effectiveness in modelling front-door adjustment via style transfer algorithms. As mentioned in Section 5, the great performance of CIRL is owing to many sub-modules apart from the causal intervention, such as the adversarial mask, while our methods learn a plain classifier with only the maximum interventional likelihood objective. This may be the reason why CIRL outperforms FAGT in *Sketch* on PACS, while our methods are competitive with CIRL in other domains.

## D EXPERIMENTAL DETAILS

We used the Pytorch Dsssl toolbox [70] with Python 3.6 and Pytorch 1.10. All experiments were conducted on an Ubuntu 20.04 server with a 20-cores CPU, 384GB RAM, and Nvidia V100 32GB GPUs. Apart from the hyper-parameters discussed in the main paper, we also consider two other hyper-parameters including: i) the content-style interpolation coefficient  $\alpha$  in Eq. (13); and ii) the coefficient  $\beta$  which trades off between the prediction of the original content image and those of multiple stylised images in Eqs. (18), (20), and (21). We used grid search on the validation set to find optimal values for  $\alpha$  and  $\beta$ , which are shown in Table 4.

	Mem (GiB)	Training (s)	Testing (s)	Acc (%)
ERM [51]	2.202	891	4	79.5
CIRL [29]	5.174	6381	243	86.3
FAST	5.542	4832	107	86.2

**Table 5: Comparison between our method FAST, a recent SOTA causality-based method CIRL [29] and ERM [51] in terms of the memory usage, total training time and testing time on PACS. From left to right columns, we report the memory usage (GiB), the training time (seconds), the testing time (seconds) and the average accuracy (%). The accuracy of baselines are referenced from [29].**

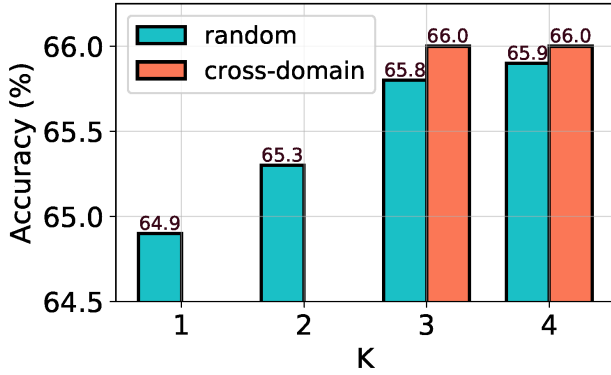


**Figure 7: Accuracies (in %) of FAST on Office-Home with different numbers of style images  $K$ . “random” and “domain-balance” denote two sampling strategies of style images.**

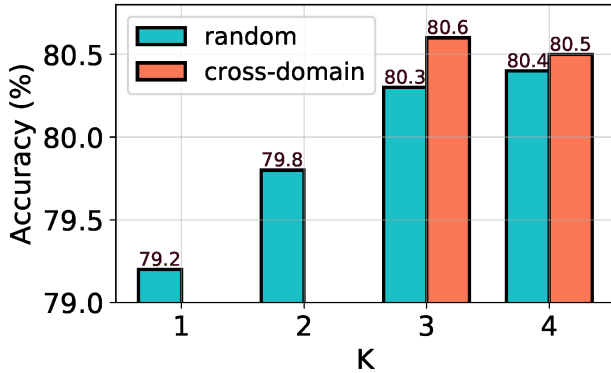


**Figure 8: Accuracies (in %) of FAST on Digits-DG with different numbers of style images  $K$ . “random” and “domain-balance” denote two sampling strategies of style images.**

## E MORE ABLATION STUDIES

### E.1 Number of style images

We also report the performance of FAST while varying the number of style images  $K$  (Eq. 18) on Office-Home [52] and Digits-DG [68] in Figures 7 and 8. Like the analysis on PACS [24] in the main paper, we observe that i) with the random sampling strategy, the results are better with larger values of  $K$ , and ii) the results are improved further when the balance in the number of sampled style images across domains is established.

### E.2 Memory Usage and Running Time

We compare our method FAST, a recent SOTA causality-based method CIRL [29], and ERM [51] in terms of the memory usage, total training time and testing time on PACS. For a fair comparison, both methods use the same GPU resources and experimental protocol (e.g., batch size) for both the training and testing phases. Results are reported in Table 5. Compared with ERM, FAST introduces 2.3 GiB memory usage, about more 4000 and 100 seconds in the training and testing phases respectively, while gaining a significant improvement of 6.7% on PACS. Although our performance remains competitive with that of CIRL, our method FAST requires much less training and testing time than CIRL, while the difference in allocated memory resources between the two methods is meager.

## F VISUALISATIONS

### F.1 Stylised images in Neural Style Transfer

We visualise stylised images produced by the AdaIN NST model of FAST on PACS, Office-Home, and Digits-DG in Figures 9, 10, and 11 respectively.

### F.2 Stylised images in Fourier-based Style Transfer

We visualise stylised images produced by the Fourier-based Style Transfer of FAST on PACS, Office-Home, and Digits-DG in Figures 12, 13, and 14 respectively.

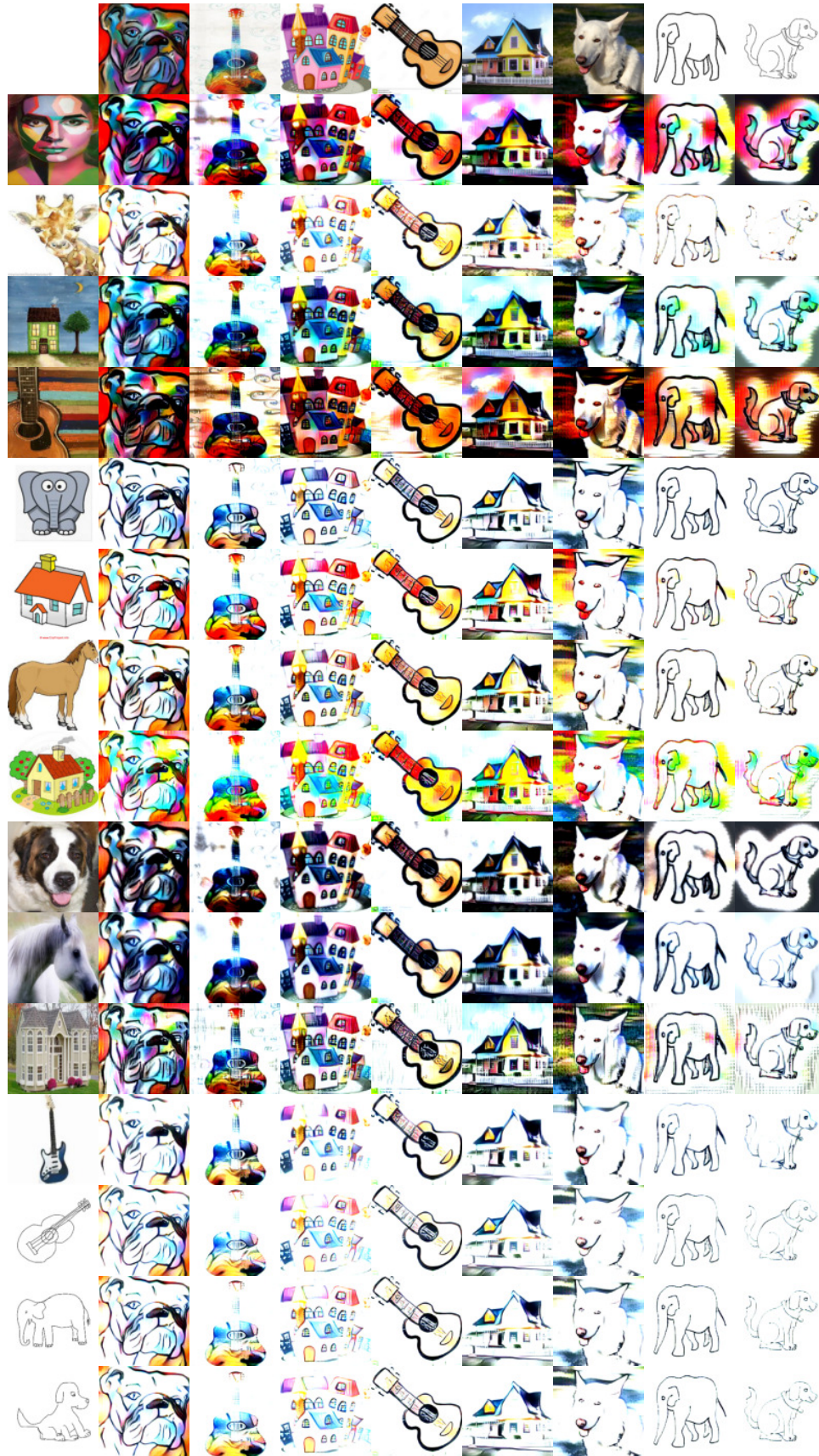


Figure 9: Stylised images produced by the AdaIN NST model of FAST on PACS with  $\alpha = 0.6$  in *Sketch* and  $\alpha = 0.75$  in the other domains. The content and style images are visualised on the first row and column respectively.





Figure 10: Stylised images produced by the AdaIN NST model of FAST on Office-Home with  $\alpha = 0.6$  in *ClipArt* and  $\alpha = 0.45$  in the other domains. The content and style images are visualised on the first row and column respectively.



Figure 11: Stylised images produced by the AdaIN NST model of FAST on Digits-DG with  $\alpha = 0.45$  in all domains. The content and style images are visualised on the first row and column respectively.



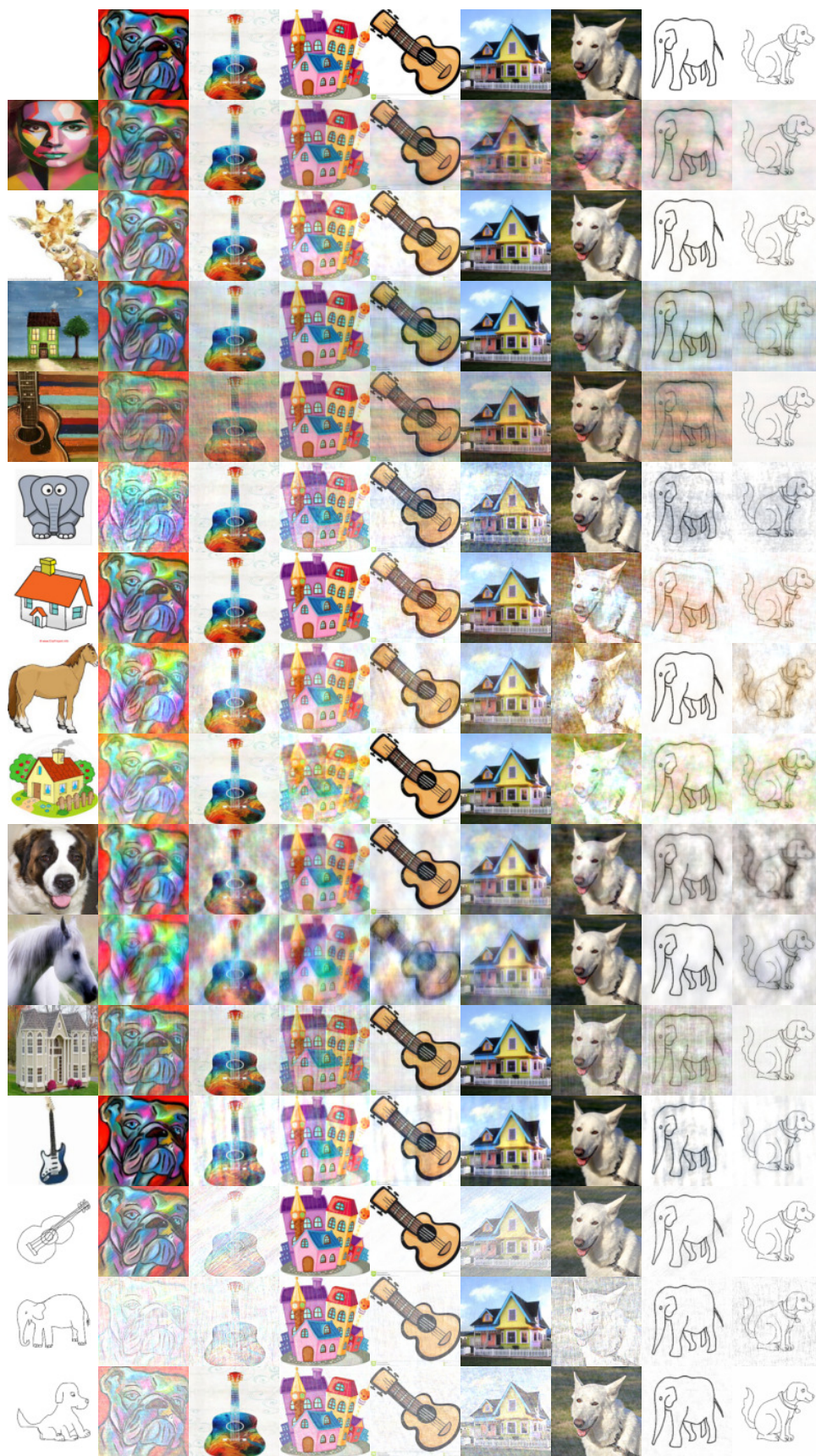


Figure 12: Stylised images produced by the Fourier-based Style Transfer of FAFT on PACS. The content and style images are visualised on the first row and column respectively.





Figure 13: Stylised images produced by the Fourier-based Style Transfer of FAFT on Office-Home. The content and style images are visualised on the first row and column respectively.





Figure 14: Stylised images produced by the Fourier-based Style Transfer of FAFT on Digits-DG. The content and style images are visualised on the first row and column respectively.